Available online at www.sciencedirect.com
SCIENCE DIRECT
International Journal of Heat and Mass Transfer 49 (2006) 2545–2556
International Journal of HEAT and MASS TRANSFER
www.elsevier.com/locate/ijhmt

Image based heating rate calculation from thermographic data considering lateral heat conduction

Malte Estorf *

Institute of Fluid Mechanics, Technical University Braunschweig, Bienroder Weg 3, 38106 Braunschweig, Germany

Received 12 August 2005; received in revised form 23 November 2005
Available online 20 March 2006

Abstract

An image based method for transient surface normal heat flux calculation from thermographic data is suggested. It is based on an analytical solution of the three-dimensional linear heat conduction equation. The method yields correct results for the surface normal heat flux even in regions with strong lateral gradients by taking into account the transient surface temperature of an area surrounding each evaluation point within the thermographic image. The solution for the heat flux can be stabilized with respect to measurement errors by an iterative regularization method. The validation of the method in synthetic test cases indicates its good accuracy over a broad range of Fourier numbers.

Keywords: Thermography; Analytical; Conduction; Inverse; Three-dimensional; Heat flux

1. Introduction

The accurate knowledge of surface heating rate is of considerable importance in many fields of thermal design. Since the surface normal heat flux is not directly accessible by measurements it has to be estimated from transient temperature measurements. The measured temperature has to be linked with the surface heat flux by solving a boundary inverse heat conduction problem. If the temperature is measured directly at the boundary, as in thermography, the problem is stated pseudo inverse [1] since it reduces to recalculating a boundary condition of the first kind into a second kind boundary condition, hence no continuation of the heat conduction equation solution is needed. There are several methods to solve this data reduction problem. The most widely applied methods have been classified and evaluated by Walker and Scott [2]. They divide the methods into three primary classes.

The first class uses closed-form solutions of the heat conduction equation to resolve the heat flux in terms of an analytical function of the measured temperature. Among those is the one-dimensional semi-infinite solid conduction method proposed by Cook and Felderman [3]. This simple method is tailored to discrete temperature sensors such as thin film gauges [4]. These are designed such that the temperature field in the sensing element may be identified with the one-dimensional temperature field in a semi-infinite solid with uniform heat flux at its surface. Thus, the method cannot account for lateral surface heat conduction and fails when it is applied on surfaces with steep gradients in the heat flux density. Moreover the class one methods are restricted to cases for which the linearized heat conduction equation applies, i.e. constant thermometric conductivity has to be assumed.

This is overcome by the class two methods which use numerical techniques to solve the conduction equation for arbitrary geometries. The measured surface temperature is applied as a boundary condition to a transient finite-element or finite-difference calculation. The surface heat flux can then be found from an energy balance at

* Tel.: +49 531 391 2975; fax: +49 531 391 5952.
E-mail address: m.estorf@tu-bs.de

0017-9310/$ - see front matter © 2006 Elsevier Ltd. All rights reserved.
doi:10.1016/j.ijheatmasstransfer.2005.12.018

Nomenclature

a	thermometric conductivity
$\underline{\underline{A}}$	transfer function
b_x, b_y	width, height of rectangular bar
c	specific heat capacity
d	distance from boundary or thickness of body
$\underline{D}$	descent direction, Eq. (37)
Fo	Fourier number
I, J, K	dimension of measured data
$\mathscr{J}$	residual functional
t	time
q	heat density
$\vec{\dot{q}} = \{\dot{q}_x, \dot{q}_y, \dot{q}_z\}^{\mathrm{T}}$	vector of heat flux density
$\dot{Q}$	substitute surface normal heat flux density, Eq. (16)
T	temperature
u, v, w	coordinates in Fourier space (cartesian wave numbers)
x, y, z	cartesian coordinates, z is the wall-normal direction

Greek symbols

α	descent parameter, Eq. (40)
β	conjugation parameter, Eq. (38)
δ	evaluation error
Δ	finite difference
$\underline{\epsilon}$	measurement error
θ	transformed temperature, Eq. (2)
Θ	substitute temperature, Eq. (19)
λ	thermal conductivity
ξ, η	transformed cartesian coordinates, Eq. (15)
ϱ	density
σ^2	variance of measurement
τ	integration time
ω	norm of wave number vector, Eq. (27)

Indices

0	initial state
f	final
e	evaluated
i	input
i, j, k	indices of measurement points (i, j: spatial; k: temporal)
l, m, n	indices of evaluation points (l, m: spatial; n: temporal)
$'$	evaluation point
v	iteration index

the surface control volume. Although the flexibility in solving the conduction equation is increased by these methods, they introduce some additional uncertainties arising from the discretization as discussed in [2].

The third class of methods is usually applied to inverse heat conduction problems where the temperature is measured in some distance from the boundary. The inherently ill-posed character of those problems implies exact solutions to be unstable. That is the calculated heat flux does not depend continuously on the measured temperature which causes heat flux estimations to be corrupted if the temperatures are subject to small measurement errors. To solve this kind of problems regularization techniques have to be applied [5]. This is done in the class three methods which most commonly solve the inverse problem based on a least-squares minimization. The solution can be found by calculating the temperature resulting from an initially assumed heat flux and comparing it to the measured temperatures. An optimization scheme involving the regularization is then used to find an updated guess for the heat flux. The subsequent forward conduction analysis can be performed by any analytical or numerical solution method. Walker and Scott have shown that these techniques can be particularly useful to solve the pseudo inverse problem treated here.

Digital thermographic imaging techniques provide time-resolved high-resolution surface temperature data which allows for heat flux analysis considering the lateral conduction. For this purpose the common class two and class three methods need a finite volume discretization of the whole body in order to solve the discretized heat conduction equation within the 3D domain. That is a considerable numerical effort if the spacial discretization of the surface heat flux is determined by the resolution of the thermographic image [6]. In order to reduce the number of unknowns the surface heat flux can be parametrized by specifying functions for its distribution in space and time which at the same time regularize the solution (e.g. [7] or [8]). Sophisticated model reduction techniques for inverse heat conduction problems have been proposed in [9] and references therein. However, all of these techniques predispose some filtering of the measured signal which is inevitable if the number of unknowns is reduced. A well directed filtering approach by parametrization of the surface heat flux with sinusoidal functions has been given in [10]. There the temperature was measured on the back of a flat plate in order to estimate the heat flux on the front surface. The discrete cosine transform of the temperature signal on the back surface was taken to identify all frequencies with amplitudes beyond some threshold. Only those frequencies were assumed to contribute to the heat flux on the front. A numerical scheme was then applied to calculate the nonlinear temperature response to each relevant Fourier component of the heat flux. The resulting sensitivity matrix was taken to calculate the heat flux on the front with Beck's [11] regularization method. It was shown, that the number

of unknowns could be significantly reduced by this procedure which solves the inverse problem only for the dominant frequencies of the thermographic images and by this filters the measurement noise efficiently.

The approach presented in this paper is a compromise between the simplicity of the class one methods and the accuracy of the class three methods at the cost of reduced flexibility concerning geometry and thermophysical properties: An analytical 3D solution of the linearized equation of heat conduction is adopted to calculate the surface normal heat flux directly from the thermographic data without the need of finite-difference modelling. Discrete data reduction schemes are developed subsequently for the evaluation of the thermographic images in Fourier space and in real (image) space. Evaluation in Fourier space involves a discrete Fourier transform (DFT) of the thermographic data which yields a spatially decoupled solution of the problem. For the real space evaluation the images are treated with Gaussian filter masks which gives substitute temperature values for each image point. This substitute temperature can then be evaluated by the formula of Cook and Felderman [3]. The amplification of measurement noise brought over by the direct solution methods can be avoided by solving for the heat flux iteratively with a conjugate gradient algorithm using a regularizing stopping criterion [12]. In case of the decoupled solution in Fourier space this stopping criterion singles out the relevant frequencies and thereby takes the role of the threshold criterion used for filtering in [10]. However, due to the analytical approach (which implies temperature independent thermophysical properties) the computational effort of the method is by some orders of magnitude smaller than for the numerical methods described in literature, hence, no model reduction is needed and all discrete frequencies of the thermographic image can be considered for the estimated heat flux if necessary.

2. Problem statement

A semi-infinite solid body ($-\infty < x,\ y < \infty;\ z \geqslant 0$) is subject to a heat flux $\dot{q}_z(x,y,z,t)|_{z=0}$ normal to the surface. Here $|_{\ldots}$ denotes the evaluation at some specific point. The temperature at the surface $T(x,y,z,t)|_{z=0}$ is supposed to be known for the time interval $0 \leqslant t \leqslant t_f$. The initial temperature of the body including its boundary for $t < 0$ is constant and can be set to zero ($T(x,y,z,t)|_{t=0} = T_0 = 0$). The unknown heat flux $\dot{q}_z(x,y,z,t)$ at any time t is to be calculated. The problem is governed by the heat conduction equation

$$c\varrho\frac{\partial T}{\partial t} = \nabla(\lambda\nabla T), \tag{1}$$

where the thermal conductivity λ, the specific heat capacity c and the density ϱ all depend on the temperature. But for many materials the thermometric conductivity $a = \lambda/(\varrho c)$ depends less on temperature than λ does. Then it is reasonable to linearize Eq. (1) by using the transformation [13]

$$\theta = \frac{1}{\lambda_0}\int_{T_0}^{\mathrm{T}} \lambda(T')\,\mathrm{d}T', \tag{2}$$

where λ_0 is the thermal conductivity at temperature T_0. The transformed temperature θ will be called only temperature in the following since it has the same dimension and is similar to the temperature in a problem with constant λ. With this simplification the governing heat conduction equation becomes

$$\frac{\partial\theta}{\partial t} = a\left(\frac{\partial^2\theta}{\partial x^2} + \frac{\partial^2\theta}{\partial y^2} + \frac{\partial^2\theta}{\partial z^2}\right). \tag{3}$$

Here a shall not depend on temperature. The initial condition stated for T holds for the transformed temperature ($\theta|_{t=0} = 0$). The heat flux in demand is the z-component of the heat flux vector defined by $\vec{q} = -\lambda_0\nabla\theta$.

3. Analytic solution

3.1. Formulation in Fourier space

The temperature field developing in an infinite solid ($-\infty < x,y,z < \infty$) from a given initial distribution $\theta|_{t=0}(x,y,z)$ can be found by transforming the temperature from real space into Fourier space [14]

$$\theta|_{t=0}(u,v,w) = \int_{-\infty}^{\infty}\int_{-\infty}^{\infty}\int_{-\infty}^{\infty}\theta|_{t=0}(x,y,z)\mathrm{e}^{-\mathrm{i}(ux+vy+wz)}\,\mathrm{d}x\,\mathrm{d}y\,\mathrm{d}z. \tag{4}$$

Now inserting any component of a Fourier series $\theta|_{u,v,w}(t)\mathrm{e}^{\mathrm{i}(ux+vy+wz)}$ into Eq. (3) one obtains

$$\frac{\mathrm{d}\theta|_{u,v,w}(t)}{\mathrm{d}t} + a(u^2+v^2+w^2)\theta|_{u,v,w}(t) = 0 \tag{5}$$

and from this the temporal dependency

$$\theta|_{u,v,w}(t) = \theta|_{u,v,w,t=0}\cdot\mathrm{e}^{-a(u^2+v^2+w^2)t}. \tag{6}$$

Assume the initial temperature distribution in real space $\theta|_{t=0}(x,y,z)$ to be zero everywhere but in the plane $z = 0$, where its value is infinite in such a way that the amount of heat per area that is concentrated in each point of the plane is $2q_z|_{z=0}(x,y)$. This can be written with the delta function $\delta(z)$

$$\theta|_{t=0}(x,y,z) = \frac{2q_z(x,y)}{\varrho c}\delta(z). \tag{7}$$

The factor 2 is used in order to identify $q_z(x,y)$ with the heat supplied to half of the body ($z \geqslant 0$). Putting Eq. (7) into Eq. (4) and using Eq. (6) one obtains with $\int\delta(z)\mathrm{e}^{-\mathrm{i}wz}\,\mathrm{d}z = 1$

$$\theta(u,v,w,t) = \frac{2}{\rho c}q_z(u,v)\cdot\mathrm{e}^{-a(u^2+v^2+w^2)t}, \tag{8}$$

where $q_z(u,v)$ is the 2D Fourier transform of the assumed heat distribution

$$q_z(u,v) = \int_{-\infty}^{\infty}\int_{-\infty}^{\infty} q_z(x,y)\cdot \mathrm{e}^{-\mathrm{i}(ux+vy)}\,\mathrm{d}x\,\mathrm{d}y. \tag{9}$$

Transforming only the third dimension back into real space yields

$$\theta(u,v,z,t) = \frac{2}{\rho c} q_z(u,v)\cdot \mathrm{e}^{-a(u^2+v^2)t}\frac{1}{2\pi}\int_{-\infty}^{\infty}\mathrm{e}^{-aw^2t}\mathrm{e}^{\mathrm{i}wz}\,\mathrm{d}w. \tag{10}$$

Because e^{-aw^2t} is an even function with respect to w the integral reduces to

$$\int_{-\infty}^{\infty}\mathrm{e}^{-atw^2}\cos(wz)\,\mathrm{d}w = \sqrt{\frac{\pi}{at}}\,\mathrm{e}^{-\frac{z^2}{4at}}. \tag{11}$$

For symmetry reason half of the heat assumed in Eq. (7) will propagate into positive z-direction. So Eq. (10) can be identified with the solution of the semi-infinite temperature field ($z \geqslant 0$) where $q_z(x,y)$ is released into the surface at time $t = 0$. The linearity of Eq. (3) allows for superposition of this solution for heat released at subsequent time steps. Thus, the Fourier transformed temperature field due to a transient heat supply $\dot{q}_z|_{z=0}(x,y,\tau)$ with $\tau \in [0 \ldots t]$ is

$$\theta(u,v,z,t) = \frac{1}{\rho c\sqrt{a\pi}}\int_0^t \dot{q}_z|_{z=0}(u,v,\tau)\frac{\mathrm{e}^{-a\left[(u^2+v^2)(t-\tau)\right]}}{\sqrt{t-\tau}}\cdot \mathrm{e}^{-\frac{z^2}{4a(t-\tau)}}\,\mathrm{d}\tau. \tag{12}$$

This is the forward solution of the heat conduction problem giving the transient temperature of the body as an integral over the history of its surface heat flux in Fourier space. For the iterative estimation of the heat flux as it is presented in Section 5 a discrete form of this equation is used. It is shown in Appendix A how the inverse of Eq. (12) can be found where the heat flux is a function of surface temperature:

$$\dot{q}_z|_{z=0}(u,v,t) = \frac{\lambda_0}{\sqrt{a\pi}}\int_0^t \frac{\partial(\theta|_{z=0}(u,v,\tau)\mathrm{e}^{-a[(u^2+v^2)(t-\tau)]})}{\partial\tau}\frac{\mathrm{d}\tau}{\sqrt{t-\tau}}. \tag{13}$$

For the constant element of the Fourier series ($u = v = 0$) Eqs. (12) and (13) reduce to the well-known one-dimensional solution.

3.2. Formulation in real space

The corresponding formulations of the direct and the inverse solutions (Eqs. (12) and (13)) in real space can be found by transformations similar to that already done for the z-component in Eqs. (10) and (11). Merely, the coordinates (x,y) are already used for localization of the released heat flux, hence (x',y') is used for the point of evaluation. With Eq. (9) this results in

$$\theta(x',y',z,t) = \int_0^t \frac{\mathrm{e}^{-\frac{z^2}{4a(t-\tau)}}}{4[\pi a(t-\tau)]^{\frac{3}{2}}\varrho c}\cdot\int_{-\infty}^{\infty}\int_{-\infty}^{\infty}\dot{q}_z|_{z=0}(x,y,\tau)\mathrm{e}^{-\frac{(x'-x)^2+(y'-y)^2}{4a(t-\tau)}}\,\mathrm{d}x\,\mathrm{d}y\,\mathrm{d}\tau. \tag{14}$$

The surface integration can be done in a time-dependent coordinate system

$$\begin{aligned}\xi &= \frac{x}{\sqrt{4a(t-\tau)}}; \quad \sqrt{4a(t-\tau)}\,\mathrm{d}\xi = \mathrm{d}x,\\ \eta &= \frac{y}{\sqrt{4a(t-\tau)}}; \quad \sqrt{4a(t-\tau)}\,\mathrm{d}\eta = \mathrm{d}y,\end{aligned} \tag{15}$$

which yields a substitute local heat flux $\dot{Q}$ for each surface point

$$\dot{Q}(x',y',t,\tau) = \frac{1}{\pi}\int_{-\infty}^{\infty}\int_{-\infty}^{\infty}\dot{q}_z|_{z=0}(\xi,\eta,\tau)\mathrm{e}^{-[(\xi'-\xi)^2+(\eta'-\eta)^2]}\,\mathrm{d}\xi\,\mathrm{d}\eta. \tag{16}$$

Introducing this in Eq. (14) and evaluation at the surface gives the surface temperature as a function of the substitute heat flux

$$\theta(x',y',t) = \frac{1}{\rho c\sqrt{\pi a}}\int_0^t \frac{\dot{Q}(x',y',t,\tau)}{\sqrt{t-\tau}}\,\mathrm{d}\tau. \tag{17}$$

The inverse form giving the surface heat flux as a function of the surface temperature can be derived accordingly from Eq. (13)

$$\dot{q}_z|_{z=0}(x,y,t) = \frac{\lambda_0}{\sqrt{\pi a}}\int_0^t \frac{\partial\Theta(x,y,t,\tau)}{\partial\tau}\frac{1}{\sqrt{t-\tau}}\,\mathrm{d}\tau \tag{18}$$

with

$$\Theta(x,y,t,\tau) = \frac{1}{\pi}\int_{-\infty}^{\infty}\int_{-\infty}^{\infty}\theta_z|_{z=0}(\xi',\eta',\tau)\mathrm{e}^{-[(\xi-\xi')^2+(\eta-\eta')^2]}\,\mathrm{d}\xi'\,\mathrm{d}\eta'. \tag{19}$$

Note that in case of uniform surface temperature and heat flux Eqs. (17) and (18) reduce to the well-known solutions of the one-dimensional problem because then it is $\dot{Q}(x',y',t,\tau) = \dot{q}_z|_{z=0}(\tau)$ and $\Theta(x,y,t,\tau) = \theta|_{z=0}(\tau)$.

3.3. Semi-infinite rectangular bar

For the solution given above a semi-infinite body has been assumed. The solution can be extended to areas that are close to straight edges with adiabatic bounding faces. In practice this condition could be realised by a rectangular surface insert mounted on an isolating material as in [6].

Assume a semi-infinite rectangular bar $0 \leqslant x \leqslant b_x$, $0 \leqslant y \leqslant b_y$, $0 \leqslant z \leqslant \infty$ with a non-uniform heat flux supplied to its surface at $z = 0$. The other four surfaces have adiabatic boundary condition. The temperature field developing in this body is that of a semi-infinite body with the surface heat flux being periodically continued over the boundaries. The corresponding semi-infinite temperature field is found by the method of images outlined in [13]. This

is illustrated in Fig. A.1. The body is continued in x- and y-direction and the heat flux at $z = 0$ is mirrored about all planes $x = s \cdot b_x$; $y = s \cdot b_y$ with $s = 0, \pm 1, \pm 2, \ldots$ The resulting temperature field is symmetric to the bounding planes and therefore there is no heat flux on the boundaries of the body except the heat supplied at $z = 0$ which is the required condition. So the heat flux on the physical surface can be evaluated by using the mirrored surface temperature field.

3.4. Plane plate of finite thickness

With Eq. (12) the temperature field caused by a heat flux at the surface $z = 0$ is given as a function of the distance z from this surface. The method of images [13] can be applied to expand this solution for the case with zero heat flux on a second surface at distance $z = d$, that is to calculate the temperature field within a plane plate of thickness d with the heat flux $\dot{q}_z|_{z=0}$ at its front surface and with adiabatic back surface. This can be modelled by placing heat sources that are mirror images of the front surface heat flux in all planes $z = 2n \cdot d$ with $n \in \mathbb{Z}$ which gives

$$\theta(u,v,z,t) = \frac{1}{\rho c\sqrt{a\pi}} \int_0^t \dot{q}_z|_{z=0}(u,v,\tau) \times \frac{\mathrm{e}^{-a[(u^2+v^2)(t-\tau)]}}{\sqrt{t-\tau}} \left(\sum_{n=-\infty}^{\infty} \mathrm{e}^{-\frac{(z-2nd)^2}{4a(t-\tau)}} \right) \mathrm{d}\tau. \tag{20}$$

In practice the number of terms that have to be included in the sum depends on the time span $(t - \tau)$. Their value soon becomes small for large n considering only the physical area $0 \leqslant z \leqslant d$. The inverse of this solution is not given, however, the preferred solution method for the inverse problem is the iterative regularization method described in Section 5 where only forward conduction analysis is needed. Note that the equation above can also be taken to find the front surface heat flux from temperature measurements at the back surface ($z = d$) as it has been done numerically for the nonlinear case in [10]. If the heat flux at the back surface is non-zero but known for example as a function of temperature, the problem can be decomposed due to the presumed linearity into a direct and an inverse problem (see [9]). Both can be solved by the equation above.

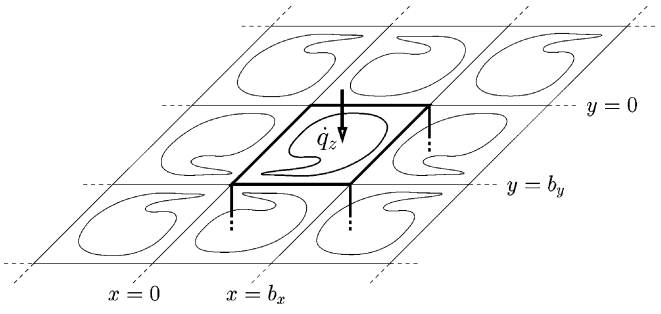

Fig. A.1. Mirrored temperature field for heat flux evaluation close to adiabatic edges of a body.

3.5. Different geometries

Most technical cases have to deal with finite body depth and different boundary types than assumed above. But the assumption of a semi-infinite body can still be reasonable for a plane surface at some distance from the edges of a finite body provided the measurement time is small compared to the time it would take a heat flux on these edges to significantly change the temperature at the point of evaluation. It might also happen that temperatures can only be measured within a finite area of a surface which causes the solution at the edge of the evaluated area to be uncertain. In the following the necessary body size and the error at the edge of a finite evaluation area are estimated. Three cases are distinguished.

3.5.1. Adiabatic boundary

A disturbing boundary in some distance from the measured surface is known to be virtually adiabatic.

Since this case can be very complex if more than one and arbitrarily shaped boundaries are considered, an error estimation can only yield the timescale within which the body can be regarded as semi-infinite. The method of images used for the derivation of Eq. (20) illustrates the influence of an adiabatic boundary. Although now boundaries are considered that are neither plane nor parallel to the evaluation plane it is reasonable to assume that the additional terms introduced by such boundaries are of the same order of magnitude. Therefore the assumption of a semi-infinite body holds as long as these additional terms are smaller than a certain percentage of the term representing the surface heat flux itself. For example if d is the smallest distance between the point of evaluation and the disturbing boundary and a 1% error in the heat flux can be allowed it has to be claimed that

$$2\sum_{n=1}^{\infty} \mathrm{e}^{-\frac{(2nd)^2}{4a(t-\tau)}} < 2\left(\mathrm{e}^{-\frac{d^2}{at}} + \frac{1}{\mathrm{e}^{\frac{4d^2}{at}} - \mathrm{e}^{-\frac{d^2}{at}}} \right) < 1\%. \tag{21}$$

For the relevant values of $d^2/at > 1$ the sum is dominated by its first term hence it is sufficient to claim

$$2\mathrm{e}^{-\frac{d^2}{at}} < 1\% \quad \text{which gives} \quad \frac{d^2}{at} > 5.3. \tag{22}$$

Thus the inverse Fourier number $Fo^{-1} = d^2/at$ built with the smallest distance between a disturbing boundary and the point of evaluation and with the measurement time has to be larger than the estimated value of 5.3. But note that in case of several disturbing boundaries some larger value has to be claimed for Fo^{-1}.

3.5.2. Non-adiabatic boundary

The heat flux on the disturbing boundary plane has the same order of magnitude as the heat flux on the evaluated plane.

With the same reasoning as before Eq. (20) is taken for a rough estimation of the necessary body size or maximum

measurement time, respectively. But now the heat flux on the disturbing surface has the same influence on the temperature at the surface of evaluation as vice versa. Therefore the terms from Eq. (20) representing the disturbing effect are evaluated for $z = d$ assuming again that d is the smallest distance between the point of evaluation and the disturbing boundary. The resulting terms have to be added to the error terms arising from the case with adiabatic boundary given above. Then the demand for less than 1% error in the heat flux evaluation becomes

$$\begin{aligned} 2\sum_{n=1}^{\infty}\left(\mathrm{e}^{-\frac{(2n-1)^2d^2}{4a(t-\tau)}}+\mathrm{e}^{-\frac{(2n)^2d^2}{4a(t-\tau)}}\right) &\leqslant 2\sum_{n=1}^{\infty}\mathrm{e}^{-\frac{n^2d^2}{4at}} \\ &< 2\left(\mathrm{e}^{-\frac{d^2}{4at}}+\frac{1}{\mathrm{e}^{\frac{d^2}{at}}-\mathrm{e}^{-\frac{d^2}{4at}}}\right) \\ &< 1\%. \end{aligned} \tag{23}$$

Again for $d^2/4at > 1$ the first term of the sum is an order of magnitude larger than the rest which gives

$$\frac{d^2}{at} = Fo^{-1} > 21.2. \tag{24}$$

With a slightly different derivation $Fo^{-1} > 16$ has been claimed in [4] for the use of the semi-infinite one-dimensional evaluation method.

3.5.3. Finite field of view

The temperature is measured far away from any boundaries but the area viewed by the camera is finite and therefore the temperature beyond the field of view is unknown and cannot be used for the evaluation of Eq. (16) or (19).

For the 3D-evaluation some assumption has to be made for the unknown temperature. If no better estimation can be found it appears reasonable for evaluation in Fourier space to assume that the temperature continues periodically over the edge of the image. For evaluation in real space one would rather set the temperature outside the measurement area to its closest measured value at the edge or take a higher order extrapolation. However, for the following estimation of the evaluation error at a distance d from the image edge it is assumed that the guessed outside temperature differs by $\pm\delta\theta$ from its real value. The error of $\Theta(d,t,\tau)$ (Eq. (19)) becomes

$$\delta\Theta(d,t,\tau) = \pm\left[\frac{1}{2}\mathrm{erf}\left(\frac{d}{\sqrt{4a(t-\tau)}}\right)\right]\cdot\delta\theta. \tag{25}$$

Putting this into Eq. (18) and integrating over time gives

$$\delta\dot{q}_z|_{z=0}(d,t) = \mp\frac{\lambda_0}{\pi}\cdot\frac{\mathrm{e}^{-\frac{d^2}{4at}}}{d}\cdot\delta\theta. \tag{26}$$

4. Discrete approximation

Digital cameras provide the surface temperature data in an orthogonal array of $I\times J$ discrete pixels referring to the coordinates (x_i, y_j), $i\in[0\ldots I-1]$, $j\in[0\ldots J-1]$ in physical space. It is assumed that the infrared image is spatially calibrated and distortion compensated such that the coordinate axes of physical space are aligned with the rows and columns of the pixels (see Refs. [15,16] for a detailed calibration method). Further it is assumed that the temperature measured by one pixel is the temperature at the pixel center bearing in mind that the measured value corresponds to the mean radiation intensity over the spatial area represented by one pixel. For evaluation in Fourier space the images have to be transformed according to common DFT- or FFT-algorithms. Note that the period type of Fig. A.1 is suited for a discrete cosine transform with the discrete frequencies

$$\omega_{ij} = \sqrt{u_i^2+v_j^2} = \sqrt{\left(\frac{\pi}{I\Delta x}\cdot i\right)^2+\left(\frac{\pi}{J\Delta y}\cdot j\right)^2}. \tag{27}$$

The data is sampled at K equidistant times t_k with $k\in[0\ldots K-1]$ and $K\cdot\Delta t = t_f$. In the following it is shown how Eqs. (12), (13), (17) and (18) can be approximated by the discrete data in order to evaluate the discrete heat flux and temperature values in real and in Fourier space. From the latter the values in real space can be found by the corresponding inverse transformation. The points of evaluation are denoted with spatial indices $l\in[0\ldots I-1]$ and $m\in[0\ldots J-1]$ and the temporal index $n\in[0\ldots K-1]$.

4.1. Temporal discretization

An approximation of Eq. (12) (for $z = 0$) can be found by dividing the integral into n time-intervals and assuming that $\dot{q}$ is piecewise constant on these

$$\theta_{lm,n} = \frac{1}{\rho c\sqrt{a\pi}}\sum_{k=0}^{n-1}\dot{q}_{lm,k}\int_{t_k}^{t_{k+1}}\frac{\mathrm{e}^{-a\omega_{lm}^2(t_n-\tau)}}{\sqrt{t_n-\tau}}\,\mathrm{d}\tau. \tag{28}$$

For the constant Fourier term $\omega_{lm} = 0$ this becomes

$$\theta_{lm,n} = \frac{2}{\rho c\sqrt{a\pi}}\sum_{k=0}^{n-1}\dot{q}_{lm,k}\left(\sqrt{t_n-t_k}-\sqrt{t_n-t_{k+1}}\right). \tag{29}$$

For $\omega_{lm}\neq 0$ the substitution $f_{lm}(\tau) = \omega_{lm}\sqrt{a(t_n-\tau)}$ results in

$$\theta_{lm,n} = \frac{1}{\lambda_0\omega_{lm}}\sum_{k=0}^{n-1}\dot{q}_{lm,k}\left(\mathrm{erf}[f_{lm}(t_k)]-\mathrm{erf}[f_{lm}(t_{k+1})]\right). \tag{30}$$

For the discretization of Eq. (13) the integral is divided in the same way and a piecewise linear temperature is assumed

$$\begin{aligned} \dot{q}_{lm,n} = \frac{\lambda_0}{\sqrt{a\pi}}\sum_{k=0}^{n-1}\int_{t_k}^{t_{k+1}}&\left[\frac{\theta_{lm,k+1}-\theta_{lm,k}}{\Delta t}\right. \\ &\left.+a\omega_{lm}^2\left(\theta_{lm,k}+\frac{\theta_{lm,k+1}-\theta_{lm,k}}{\Delta t}(\tau-t_k)\right)\right]\frac{\mathrm{e}^{-a\omega_{lm}^2(t_n-\tau)}}{\sqrt{t_n-\tau}}\,\mathrm{d}\tau. \end{aligned} \tag{31}$$

For the constant Fourier term with $\omega_{lm} = 0$ this becomes

$$\dot{q}_{lm,n} = \frac{2\lambda_0}{\sqrt{\pi a}} \sum_{k=0}^{n-1} \frac{\theta_{lm,k+1} - \theta_{lm,k}}{\sqrt{t_n - t_{k+1}} + \sqrt{t_n - t_k}}. \tag{32}$$

This is the formula of Cook and Felderman. For all other ω_{lm} the substitution with f from above and the use of $2\int f^2 \exp(-f^2)\,\mathrm{d}f = -f\exp(-f^2) + \int \exp(-f^2)\,\mathrm{d}f$ gives after some rearrangement

$$\begin{aligned}\dot{q}_{lm,n} = \lambda_0 \sum_{k=0}^{n-1} \Bigg\{ &\left[\left(\frac{1}{2\omega_{lm} a} + \omega_{lm}(t_n - t_k) \right) \frac{\theta_{lm,k+1} - \theta_{lm,k}}{\Delta t} \right. \\ &\left. + \omega_{lm}\theta_{lm,k} \right] \cdot \left(\mathrm{erf}[f_{lm}(t_k)] - \mathrm{erf}[f_{lm}(t_{k+1})] \right) \\ &+ \frac{\theta_{lm,k+1} - \theta_{lm,k}}{\sqrt{\pi a}\Delta t} \left(\sqrt{t_n - t_k}\, \mathrm{e}^{-a\omega_{lm}^2 (t_n - t_k)} \right. \\ &\left. - \sqrt{t_n - t_{k+1}}\, \mathrm{e}^{-a\omega_{lm}^2 (t_n - t_{k+1})} \right) \Bigg\}. \end{aligned} \tag{33}$$

For the solution in real space Eqs. (29) and (32) are used with the substitute heat flux $\dot{Q}_{lm,k}$ and temperature $\Theta_{lm,k}$ instead of $\dot{q}_{lm,k}$ and $\theta_{lm,k}$ respectively. Note that the assumption of piecewise linear Θ results in smaller limits of the time interval than assuming a linear change of temperature since the spatial integral (Eq. (19)) changes its value exponentially in regions of non-uniform heat flux. This is one of the drawbacks of the solution in real space.

4.2. Spatial discretization

The spatial discretization in Fourier space is done by the discrete Fourier transform of the images which is described in detail in pertinent textbooks (e.g. [16]) and is therefore not treated here. In the following it is shown how the surface integrations of Eqs. (16) and (19) can be performed over the discrete data. In digital image processing the method is known as a convolution operation with a Gaussian filter mask.

The evaluation is performed using a Gauss–Hermite quadrature [17] in two dimensions. This requires for each time step t_k ($k < n$), the transformation of the surface data into a local system of coordinates around the pixel at (ξ, η). The distance between two pixels in terms of $\Delta\xi'$ and $\Delta\eta'$ depends on $(n - k)$ and determines the size of the area of surrounding pixels that have to be considered for the integration at each timestep. This area decreases for $t_k \to t_n$ because physically the area that significantly influences the temperature at the point of interest decreases with time. This can be seen from Eq. (8) by deriving that $\frac{\Delta\xi'}{\Delta x'}, \frac{\Delta\eta'}{\Delta y'} \to \infty$ for $\tau \to t$. Having identified a quadratic area of $P \times P$ pixels for integration the abscissas $X_{[1\ldots P]}$ and weights $W_{[1\ldots P]}$ of the P-point Gauss–Hermite quadrature are taken to build a quadratic matrix $W_o W_p$ of the weights. Afterwards, the values from the pixels of interest are interpolated in the points ($\xi_o = X_o$; $\eta_p = X_p$). For the results presented in this paper a successive third order polynomial interpolation in the two directions was implemented. The Lagrange interpolation weights and the Hermite weights can be combined in a filter mask. The elements of the corresponding $P \times P$ data field are multiplied with elements of the mask and summed up to the value of Θ_{lm} or $\dot{Q}_{lm}$ at the center of the matrix. For better clarity Fig. A.2 shows the supporting points of the Gauss–Hermite quadrature within the square grid of pixels for the case $P = 5$. In each point the data is interpolated from 4×4 surrounding pixels. The values are then weighted and summed up to the substitute temperature or heat flux at the shaded pixel. Note that when the area of integration is growing with $(t_n - t_k)$ the integral will be approximated using more supporting points.

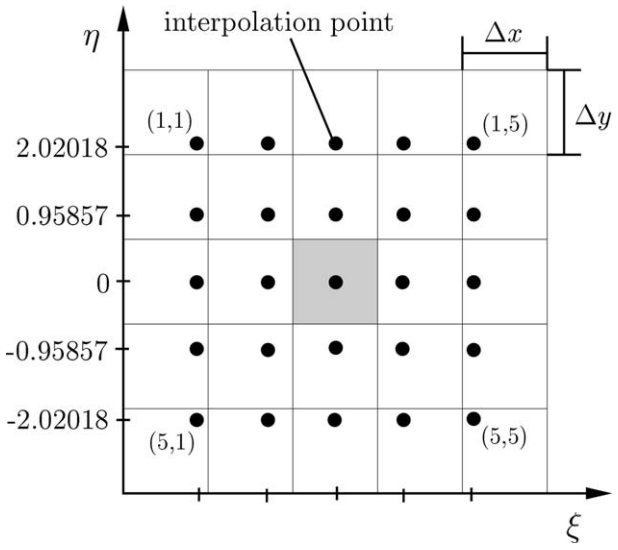

Fig. A.2. Illustration of a five-point Gauss–Hermite integration in two directions within the square grid of pixels. The weight at each interpolation point (o,p) is a product of the two hermite weights W_o and W_p.

4.3. Computational effort

Since Eqs. (29), (30), (32) and (33) as well as the spatial integration described above and the Fourier transformation are all linear operations with respect to the unknowns the direct and the inverse solution can be written as

$$\text{(a)}\ \underline{\theta} = \underline{\underline{A}} \cdot \underline{\dot{q}_z} \quad \text{and} \quad \text{(b)}\ \underline{\dot{q}_z} = \underline{\underline{A}}^{-1} \cdot \underline{\theta}. \tag{34}$$

Here $\underline{\theta}$ denotes the vector of all given temperature values and $\underline{\dot{q}_z}$ is the vector of the heat flux values to be calculated. The notation $\underline{\underline{A}}^{-1}$ indicates the inverse problem. Note that the assumption of piecewise linear temperature is not in accordance with piecewise constant heat flux which was assumed for the calculation of these matrices. Hence, here $\underline{\underline{A}}^{-1}$ is not exactly the inverse of $\underline{\underline{A}}$. For the iterative procedure described in the following section the direct problem is solved several times. Therefore the computational effort has to be considered.

The dimension of the transfer matrix $\underline{\underline{A}}$ is $(IJK)^2$ which is too big to store it in memory for usual image sizes even if only few measurements are taken in time. But if $\underline{\dot{q}_z}$ and $\underline{\theta}$ are sorted with respect to time $\underline{\underline{A}}$ is triangular and moreover its elements $\partial\theta_{lmn}/\partial\dot{q}_{ijk}$ do only depend on $(l - k)$ rather than on l and k. So only $(IJ)^2 K$ values have to be stored.

But still the computational effort in real space is of the order $\mathcal{O}[(IJK)^2]$ because in the worst case of large conductivity or large measurement time the temperature in each point depends on the past temperatures in all other points.

In contrast the solution in Fourier space is spatially decoupled because the Fourier members are eigenfunctions of the problem. So once the transform has been calculated the computational effort is only of order $\mathcal{O}[(IJ)K^2]$ and the problem can be solved sequentially for each frequency ω_{lm}, hence only K different values $\partial\theta_{lmn}/\partial\dot{q}_{lmk}$ have to be kept in memory. This advantage of the solution in Fourier space is particularly useful for the iterative solution described in the following section since the additional effort of the Fourier transformation can be neglected regarding the overall computational effort.

5. Iterative regularization

In practice the measured temperature values are subject to measurement noise. With the unknown vector of measurement errors $\underline{\epsilon}$ the vector of all measured values is $\underline{\theta}_{\text{meas}} = (\underline{\theta} + \underline{\epsilon})$. The use of finite differences of the measured values in Eqs. (32) and (33) sensitizes the inverse solution to those errors. It is easy to see from these equations that for very high sampling rates ($\Delta t \to 0$) the measurement errors can produce large errors in the determined heat flux. The aim of regularization is to find approximate solutions for the heat flux which are stable with respect to measurement errors [5]. The conjugate gradient method with a regularizing stopping criterion is known to be an effective way of finding such quasi-solution. The method is extensively described in [1,12,18]. It has been successfully applied to different inverse heat conduction problems e.g. [19,20]. The reader is also referred to [21] which is an introduction to the conjugate gradient method.

Since the direct solution (Eqs. (29) and (30)) is stable due to the determinacy of the physical problem it can be used to find a solution of the inverse problem in an iterative procedure by minimizing the functional

$$\mathscr{J}(\underline{\dot{q}}_z^v) = |\underline{\underline{A}} \cdot \underline{\dot{q}}_z^v - (\underline{\theta} + \underline{\epsilon})|^2. \tag{35}$$

v is the iteration index and $||^2$ denotes the scalar product $\sum()^2_{ijk}$. Starting from an initial guess the heat flux is corrected at each iteration into the descent direction $\underline{D}^v$

$$\underline{\dot{q}}_z{}^{v+1} = \underline{\dot{q}}_z^v + \alpha^v \underline{D}^v. \tag{36}$$

α^v is the descent parameter scaling the step-size. The descent direction is found by conjugation of the residual functional gradient $\nabla\mathscr{J}(\underline{\dot{q}}_z^v)$ at each iteration with the former direction

$$\underline{D}^v = -\nabla\mathscr{J}(\underline{\dot{q}}_z^v) + \beta^v \underline{D}^{v-1}. \tag{37}$$

β^v is the conjugation parameter. Here the Fletcher-Reeves version of the parameter is used

$$\beta^v = \frac{|\nabla\mathscr{J}(\underline{\dot{q}}_z^v)|^2}{|\nabla\mathscr{J}(\underline{\dot{q}}_z{}^{v-1})|^2}. \tag{38}$$

The residual functional gradient is found by differentiating Eq. (35) with respect to $\underline{\dot{q}}_z$

$$\nabla\mathscr{J}(\underline{\dot{q}}_z^v) = 2\underline{\underline{A}}^{\mathrm{T}}(\underline{\underline{A}} \cdot \underline{\dot{q}}_z^v - (\underline{\theta} + \underline{\epsilon})). \tag{39}$$

After the descent direction has been calculated the descent parameter α can be calculated by finding the minimum point of $\mathscr{J}$ along the direction $\underline{D}^v$. Differentiating the new residual functional $\mathscr{J}(\underline{\dot{q}}_z^v + \alpha\underline{D}^v)$ with respect to α and equating the gradient zero yields

$$\alpha^v = -\frac{(\underline{\underline{A}} \cdot \underline{D}^v)^{\mathrm{T}}(\underline{\underline{A}} \cdot \underline{\dot{q}}_z^v - (\underline{\theta} + \underline{\epsilon}))}{|\underline{\underline{A}} \cdot \underline{D}^v|^2}. \tag{40}$$

The method described so far is a standard approach [21] to solve Eq. (34b) for $(\underline{\theta} + \underline{\epsilon})$ in a least square sense and if $\underline{\underline{A}}$ is non-singular it will converge to the direct solution (with amplified noise) if no regularization is introduced. However, one can see from Eq. (35) that the value of the residual functional should never fall below $|\underline{\epsilon}|^2$ if $\underline{\dot{q}}_z^v$ solves Eq. (34a) for $\underline{\theta}$. This can be used for regularization by stopping the iteration when $\mathscr{J}(\underline{\dot{q}}_z^v) \leqslant |\underline{\epsilon}|^2$. The unknown value $|\underline{\epsilon}|^2$ is related to the variance σ^2 of the measured temperatures. The latter could be estimated from the Gaussian distribution of a reference measurement at constant temperature. Assuming that the variance is identical for each pixel and at all times the stopping criterion for the evaluation in real space becomes $\mathscr{J}(\underline{\dot{q}}_z^v) \leqslant IJK \cdot \sigma^2$. If it is further assumed that the noise is uncorrelated in space and provided that the DFT is applied in a form with an orthogonal transformation matrix the temperatures in Fourier space will have the same variance as in real space. Thus for the spatially decoupled treatment of the problem in Fourier space the stopping criterion at each frequency is $\mathscr{J}(\underline{\dot{q}}_{zlm}^v) \leqslant K \cdot \sigma^2$.

6. Results

The capabilities of the method are illustrated in three steps: First the ability to resolve spatial gradients of the surface heat flux is analysed. Then it is shown how temporal changes of the heat flux are resolved, and finally the method is applied to noisy data. All test cases are generated synthetically, which is common practice for the evaluation of data reduction schemes. However, it should be mentioned that in case of real experimental data the accuracy is usually reduced.

6.1. Spatial gradients

The heated half-plane at the surface of a semi-infinite body with a steady heat supply $\dot{q}_z$ for $0 < \tau < t$ over the area $x < 0$; $-\infty < y < \infty$ is taken as a suitable test case with an infinitely large lateral gradient of heat flux. The analytic solution of the transient surface temperature for this case is given in [13]. It has been used to generate synthetic thermographic data by setting the temperature at a pixel to the exact value calculated at its center. In reality the measured value will correspond to the mean of radiation intensity

over the pixel which is a nonlinear function of temperature; this is not modelled here. The physical problem has no characteristic length-scale and therefore the only length-scale that has to be considered is the pixel size Δx. It is used to non-dimensionalize the time from the onset of heat flux giving the Fourier number $Fo = a \cdot t/\Delta x^2$. This parameter determines the number of pixels that are significantly affected by the conduction, thus the spatial resolution of the process is determined with Fo. The temporal resolution is represented by $\Delta Fo = a \cdot \Delta t/\Delta x^2$. Fo and ΔFo are linked by the number of samples $n = t/\Delta t$ which affects the decay of the evaluation error after some change of heat flux that is discretized by linearly varying temperature or heat flux. In [3] it has been shown that in case of a step in surface heat flux Eq. (32) approximates Eq. (18) to an accuracy better than 0.5% after $n = 10$ timesteps. Thus for all results presented in this subsection $n \geqslant 10$ was selected in order to eliminate the influence of that parameter. Further a non-dimensional heat flux can be defined as $\dot{q}^* = \dot{q}_z c \Delta t^2/(\lambda \Delta x)$. For a given Fourier number the error of the evaluated heat flux $\dot{q}_e^*$ is proportional to the heat flux input $\dot{q}_i^*$, because the surface temperature which linearly enters Eq. (32) scales with this quantity in case of constant Fourier number. Therefore $\dot{q}_i^* = 100$ can be chosen which gives the error of the heat flux calculation $\delta\dot{q}^* = \dot{q}_e^* - \dot{q}_i^*$ in percent.

Fig. A.3 shows the results of heat flux evaluation for ($Fo = 2.5$; $\Delta Fo = 0.1$) with the 1D Cook–Felderman method (a) and with the presented 3D methods directly evaluated in Fourier space (b) and in real space (c). The edge of the heated area has been aligned with the edge of a pixel row, the vertices of the shown grid represent the pixel centers. The heat flux computed with the 1D method is obviously corrupted at the edge of the heated area by the lateral heat flux while the 3D methods are capable of resolving the edge with very small error. The solution in Fourier space shows small oscillations which is due to the approximation of the step by a finite number of Fourier terms. Figs. A.4(a) and (b) show how the error at the first pixel bordering the step depends on the parameters ΔFo and Fo for the different evaluation schemes. Apparently, the error of both evaluation methods in Fourier space is almost independent of Fo and ΔFo. This means that the error of these methods depends mainly on how good the heat flux distribution can be represented by a Fourier series. On the other hand the quality of the solutions evaluated in real space depends strongly on ΔFo which is due to the assumption of piecewise constant $\dot{Q}$ (iterative solution) or piecewise linear Θ (direct solution) respectively. However, the iterative method performs slightly better and its error is independent of ΔFo for small values. For $\Delta Fo > 0.1$ the error increases which means that the temporal resolution is not appropriate for the desired spatial resolution. Therefore, in practice some spatial smoothing of the data could be allowed in order to reduce the noise level without loss of the information evaluable with this scheme. For the direct evaluation method in real space ΔFo should

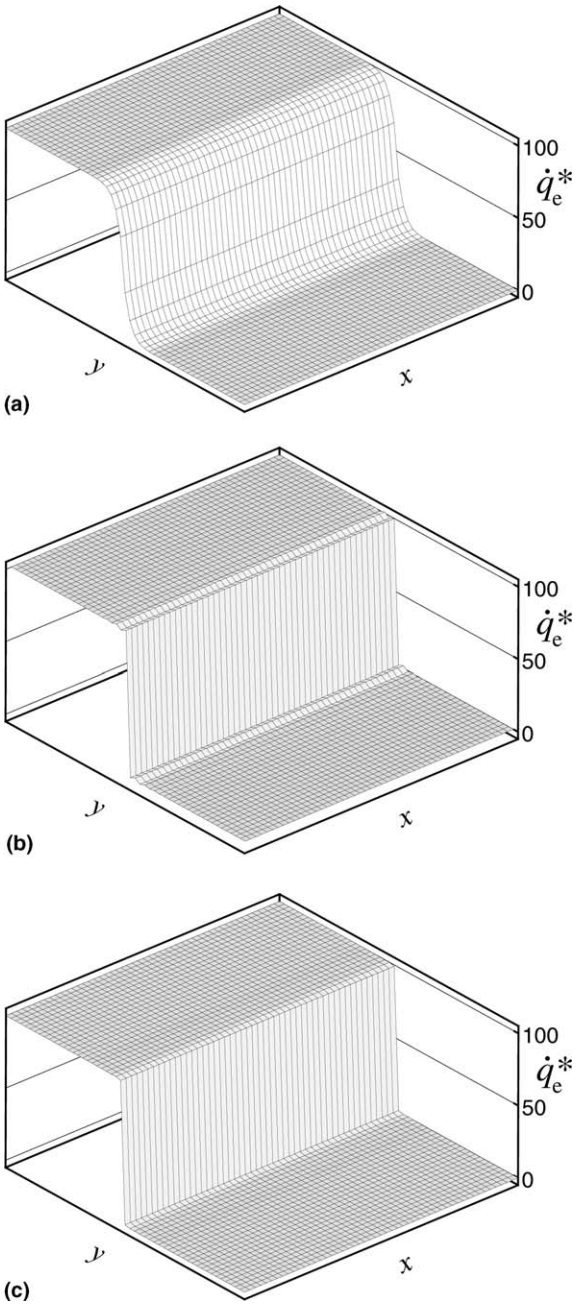

Fig. A.3. Evaluated heat flux distribution at the edge of a heated area on a semi-infinite solid ($\Delta Fo = 0.1$; $Fo = 2.5$; $\dot{q}_i^* = 100$). (a) 1D (Cook and Felderman), (b) 3D direct evaluation in Fourier space and (c) 3D direct evaluation in real space.

be within 0.05 and 0.15 for good results. The lower subfigure displays the evaluation error dependency on Fo when ΔFo is constant ($\Delta Fo = 0.005$). For the direct method in real space the small ΔFo results in comparatively large error that depends little on Fo. The iterative solution with surface integration in real space fails for large Fourier numbers. This is due to the integration procedure which for $Fo \geqslant 6$ starts skipping every second pixel around each evaluation point because the first abscissa even of the 100-point Gauss–Hermite quadrature becomes bigger than the

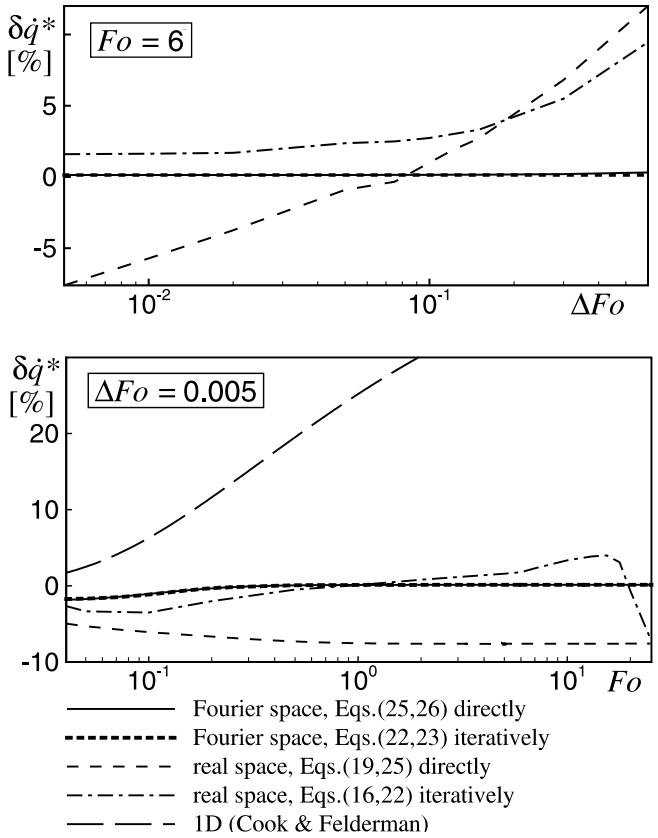

Fig. A.4. Error of the heat flux at the pixel bordering the step evaluated with different schemes depending on ΔFo and Fo.

pixel distance in terms of $\Delta\xi$ and $\Delta\eta$. This causes some high frequency eigenfunctions to be undamped during the iterative process.

6.2. Unsteady heat flux

The performance of the method for resolving temporal changes of the heat flux is tested for the same case as above but now for a fixed timestep size ($\Delta Fo = 0.1$) and for a time-dependent heat flux. A step- and a peak-shaped variation of heat flux over time have been prescribed with the heat flux changing discontinuously or proportionally to $\sqrt{t}$ within one timestep. The maximum input heat flux was $\dot{q}_i^* = 100$. Fig. A.5 shows the results of the evaluation with the 1D method and with the 3D method (solution in Fourier space) calculated directly from Eqs. (32) and (33) and iteratively from Eqs. (29) and (30). For the graphs on the left side the input heat flux changes discontinuously and on the right side it changes proportionally to the square root of time in order to meet the assumption of linearly varying temperature. Both 3D approaches outperform the 1D method at the step. The differences between the direct and the iterative solution result from the slightly different modelling assuming piecewise linear variation of temperature or piecewise constant heat flux respectively. Hence the evaluation error depends much on the physical process that is to be analysed and on the temporal offset between the measurement times and any stepwise change of heat flux as for example at the sudden onset of flow in most hypersonic windtunnels. For cases with a smooth change of heat flux with respect to the sampling rate the models assuming linear temperature and linear heat flux should perform similarly well.

6.3. Noisy data

White Gaussian noise has been added to the exact temperature data of the heated half plane described in Section 6.1. The standard deviation of the noise was chosen to be 1% of the maximum surface temperature at the time evaluated in Fig. A.6. The evaluation was done in Fourier space with the direct solution in the left subfigure and iteratively with the regularizing stopping criterion in the right figure. The regularization method yields a smoother estimate of the heat flux as has been described in the literature cited previously. The standard deviation of the evaluated heat flux is 8.5% for the direct solution and 2.5% with the regularized solution. In this particular case the computation time for the iterative solution was about 15% longer than that of the direct solution because for most of the frequencies the stopping criterion was already reached after one iteration and only some dominant frequencies needed up to six iterations. However the overall computation time for this case with 50×50 pixels and 40 timesteps was only about 8 s on a Pentium4 PC.

7. Conclusions

An analytical solution of the linearized heat conduction equation is adopted to develop data reduction schemes for the calculation of transient surface heat flux from thermographic images. The schemes account for lateral heat conduction either by calculating a substitute temperature for each image point from an integral over the surrounding surface temperature or by transforming the images into Fourier space and thereby decoupling the problem spatially. In both cases the heat flux can be computed directly or iteratively using a conjugate gradient algorithm. The latter allows to introduce a regularizing stopping criterion which avoids an amplified transmission of measurement noise to the evaluated heat flux values. The accuracy of the solution in real space was found to depend strongly on the Fourier number built with the pixel spacing and the time delay between two measurements whereas the solution method in Fourier space performed widely independent from these values. Moreover, the iterative solution method in real space becomes an unacceptable computational effort already at moderate image sizes arising from the spatial coupling. Once the discrete Fourier transform of the images has been calculated, the additional effort for the iterative solution in Fourier space is acceptable

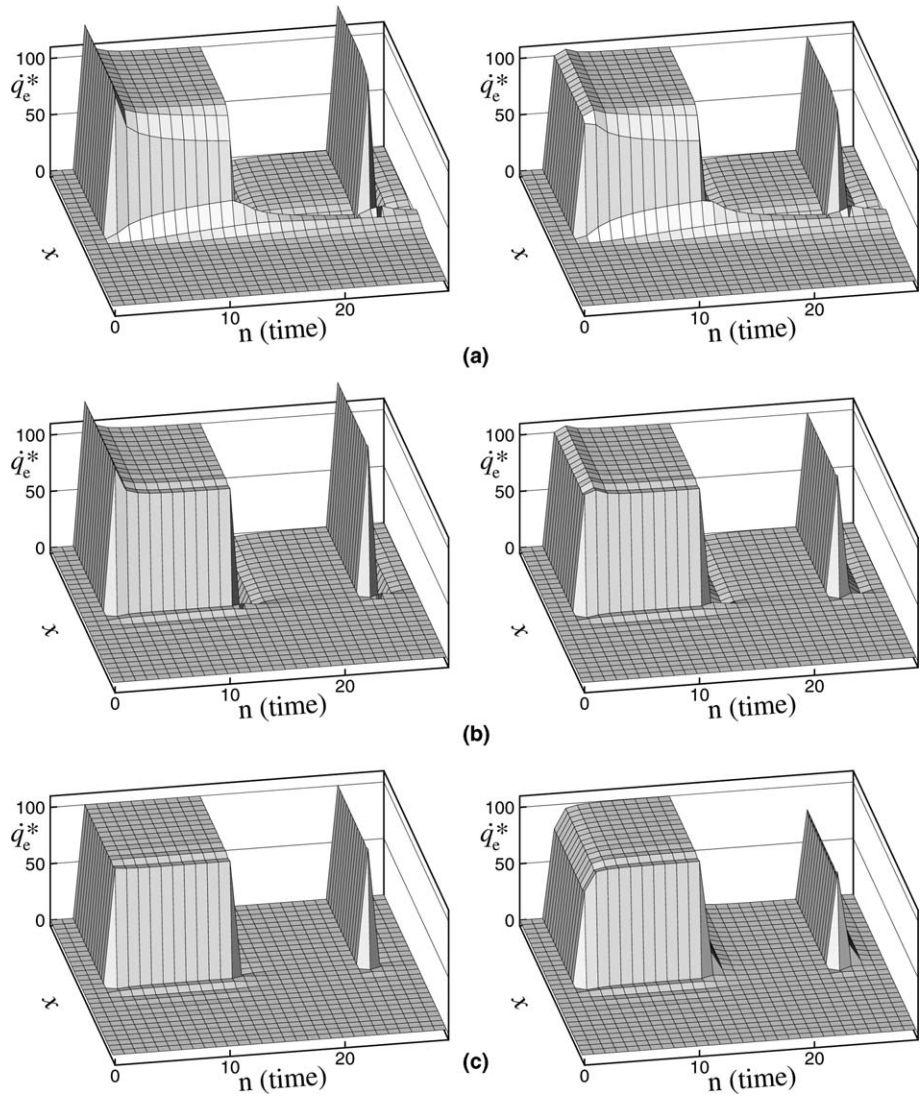

Fig. A.5. Evaluated heat flux distribution at the edge of an area with unsteady heating. The input heat flux between the timesteps was changed discontinuously in time and proportionally to the square root of time in the left and the right array of subfigures respectively ($\Delta Fo = 0.1$; $\dot{q}^*_{i,\max} = 100$). (a) 1D method; (b) 3D method, direct solution; (c) 3D method, iterative solution.

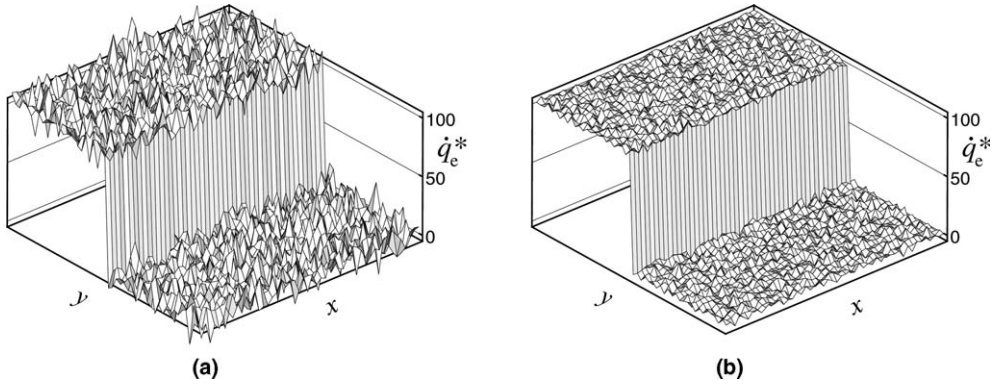

Fig. A.6. Evaluated heat flux with 1% standard deviation noise added to the temperature data ($\Delta Fo = 0.1$; $Fo = 2.5$). (a) Direct solution; (b) iterative solution.

and gives accurate results with comparatively low noise level. Therefore this solution method is preferred over the method in real space. Both methods are developed for the plane surface of a semi-infinite body or a plate of finite thickness with rectangular adiabatic edges. For different type boundaries the accuracy of the method is acceptable if the Fourier number built with the observation time and the distance of the boundary is below an estimated value. The methods can also be considered as an engineering approach for the heat flux evaluation on slightly curved surfaces if the Fourier number built with the observation time and the curvature radius is small.

Appendix A

The following steps show how Eq. (12) can be inverted. Differentiation with respect to z and multiplication with $-\lambda_0$ yields:

$$-\lambda_0 \frac{\partial\theta(u,v,z,t)}{\partial z} = \frac{z}{2\sqrt{a\pi}} \int_0^t \dot{q}_z|_{z=0}(u,v,\tau) \frac{\mathrm{e}^{-a(u^2+v^2)(t-\tau)}}{(t-\tau)^{\frac{3}{2}}} \cdot \mathrm{e}^{-\frac{z^2}{4a(t-\tau)}} \mathrm{d}\tau.$$

It can be shown by differentiation of Eq. (3) that θ and $\dot{q}_z = -\lambda_0 \frac{\partial\theta}{\partial z}$ satisfy the same differential equation. If the initial and boundary conditions of θ are also assumed for $\dot{q}_z$ (especially $\dot{q}_z(x,y,z,\tau) = 0$ for $\tau < 0$)[1] the equation above holds true when $-\lambda_0 \frac{\partial\theta(u,v,z,t)}{\partial z}$ is substituted by $\theta(u,v,z,t)$ and $\dot{q}_z|_{z=0}(u,v,\tau)$ by $\theta|_{z=0}(u,v,\tau)$:

$$\theta(u,v,z,t) = \frac{z}{2\sqrt{a\pi}} \int_0^t \theta|_{z=0}(u,v,\tau) \frac{\mathrm{e}^{-a(u^2+v^2)(t-\tau)}}{(t-\tau)^{\frac{3}{2}}} \cdot \mathrm{e}^{-\frac{z^2}{4a(t-\tau)}} \mathrm{d}\tau.$$

This is the transient temperature of the body formulated by the history of its surface temperature. Differentiating this equation another time with respect to z and again multiplying with $-\lambda_0$ gives

$$\dot{q}_z(u,v,z,t) = \frac{z^2\rho c}{4\sqrt{a\pi}} \int_0^t \theta|_{z=0}(u,v,\tau) \frac{\mathrm{e}^{-a(u^2+v^2)(t-\tau)}}{(t-\tau)^{\frac{5}{2}}} \cdot \mathrm{e}^{-\frac{z^2}{4a(t-\tau)}} \mathrm{d}\tau - \frac{\lambda_0}{2\sqrt{a\pi}} \int_0^t \theta|_{z=0}(u,v,\tau) \frac{\mathrm{e}^{-a(u^2+v^2)(t-\tau)}}{(t-\tau)^{\frac{3}{2}}} \cdot \mathrm{e}^{-\frac{z^2}{4a(t-\tau)}} \mathrm{d}\tau.$$

Finally, by integrating the second summand over τ by parts (using $T_0 = 0$) and evaluation at the surface ($z = 0$) this can be reduced to Eq. (13).

[1] It would be sufficient to claim $\dot{q}_z(x,y,z,\tau) = \text{const}$ for $\tau < 0$ but then the heat flux in demand would be $\tilde{\dot{q}}_z = \dot{q}_z - \text{const}$. To simplify notation this case is not treated here.

References

[1] O.M. Alifanov, Inverse Heat Transfer Problems, Springer, Berlin, Heidelberg, 1994.
[2] D.G. Walker, E.P. Scott, Evaluation of estimation methods for high unsteady heat fluxes from surface measurements, J. Thermophys. Heat Transfer 12 (1998) 543–551.
[3] W.J. Cook, E.J. Felderman, Reduction of data from thin-film heat-transfer gages: A concise numerical technique, AIAA J. 4 (1966) 561–562.
[4] D.L. Schultz, T.V. Jones, Heat-transfer measurements in short-duration hypersonic facilities, Tech. Rep. AGARD-AG-165, AGARDograph No. 165, 1973.
[5] A.N. Tikhonov, V.Y. Arsenin, Solutions of Ill-posed Problems, V.H. Winston & Sons, Washington, DC, 1977.
[6] K. Daryabeigi, S.A. Berry, T.J. Horvarth, R.J. Norwak, Finite volume numerical methods for aeroheating rate calculations from infrared thermographic data, AIAA Paper 2003-3634, 2003.
[7] M. Imber, Temperature extrapolation mechanism for two-dimensional heat flow, AIAA J. 12 (1974) 1089–1093.
[8] S.K. Kim, J.-S. Lee, W.I. Lee, A solution method for a nonlinear three-dimensional inverse heat conduction problem using a sequential gradient method combined with cubic-spline function specification, Numer. Heat Transfer, Part B 43 (2003) 43–61.
[9] T. Lüttich, A. Mhamdi, W. Marquardt, Design, formulation and solution of multi-dimensional inverse heat conduction problems, Numer. Heat Transfer, Part B: Fundam. 47 (2) (2005) 111–133.
[10] P. Reulet, D. Nortershauser, P. Millan, Inverse method using infrared thermography for surface temperature and heat flux measurements, in: 20th International Congress on Instrumentation in Aerospace Simulation Facilities, ICASF'03, 2003, pp. 118–126.
[11] J.V. Beck, B. Blackwell, C.R.S. Clair, Inverse Heat Conduction, Wiley-Interscience, New York, 1985.
[12] O.M. Alifanov, E.E. Artyukhin, S.V. Rumyantsev, Extreme Methods for Solving Ill-posed Problems and theirs Application to Inverse Heat Transfer Problems, Begell House, New York, 1995.
[13] H.S. Carslaw, J.C. Jaeger, Conduction of Heat in Solids, second ed., Oxford University Press, Oxford, New York, 1959.
[14] L.D. Landau, E.M. Lifshitz, Fluid Mechanics, Course of Theoretical Physics, vol. 6, Pergamon Press, London, New York, 1959.
[15] K. Ehrenfried, Processing calibration grid images using the Hough transformation, Meas. Sci. Technol. 13 (2002) 975–983.
[16] B. Jähne, Digital Image Processing, sixth ed., Springer, Berlin, Heidelberg, New York, 2005.
[17] M. Abramowitz, I.A. Stegun, Handbook of Mathematical Functions, Dover Publications Inc., New York, 1964.
[18] Y. Jarny, M.N. Ozisik, J.P. Bardon, A general optimization method using adjoint equation for solving multidimensional inverse heat conduction, Int. J Heat Mass Transfer 34 (1991) 2911–2919.
[19] C.-H. Huang, S.-P. Wang, A three-dimensional inverse heat conduction problem in estimating surface heat flux by conjugate gradient method, Int. J Heat Mass Transfer 42 (1999) 3387–3403.
[20] T. Loulou, E.P. Scott, Estimation of 3-dimensional heat flux from surface temperature measurements using an iterative regularization method, Heat Mass Transfer 39 (2003) 435–443.
[21] J.R. Shewchuck, An introduction to the conjugate gradient method without the agonizing pain. Available from: <http://www.cs.cmu.edu/~quake-papers/painless-conjugate-gradient.pdf>, 1994.